Use of Size and a Copolymer Design Feature To Improve the Biodistribution and the Enhanced Permeability and Retention Effect of Doxorubicin-Loaded Mesoporous Silica Nanoparticles in a Murine Xenograft Tumor Model

Huan Meng,[†,#] Min Xue,[‡,#] Tian Xia,[†] Zhaoxia Ji,[§] Derrick Y. Tarn,[‡] Jeffrey I. Zink,[‡,§,*] and Andre E. Nel[†,§,*]

[†]Division of NanoMedicine, Department of Medicine, University of California, Los Angeles, California, United States, [‡]Department of Chemistry & Biochemistry, University of California, Los Angeles, California, United States, and [§]California NanoSystems Institute, University of California, Los Angeles, California, United States.
[#] These authors contributed equally to this work.

ABSTRACT A key challenge for improving the efficacy of passive drug delivery to tumor sites by a nanocarrier is to limit reticuloendothelial system uptake and to maximize the enhanced permeability and retention effect. We demonstrate that size reduction and surface functionalization of mesoporous silica nanoparticles (MSNP) with a polyethyleneimine–polyethylene glycol copolymer reduces particle opsonization while enhancing the passive delivery of monodispersed, 50 nm doxorubicin-laden MSNP to a human squamous carcinoma xenograft in nude mice after intravenous injection. Using near-infrared fluorescence imaging and elemental Si analysis, we demonstrate passive accumulation of ~12% of the tail vein-injected particle load at the tumor site, where there is effective cellular uptake and the delivery of doxorubicin to KB-31 cells. This was accompanied by the induction of apoptosis and an enhanced rate of tumor shrinking compared to free doxorubicin. The improved drug delivery was accompanied by a significant reduction in systemic side effects such as animal weight loss as well as reduced liver and renal injury. These results demonstrate that it is possible to achieve effective passive tumor targeting by MSNP size reduction as well as by introducing steric hindrance and electrostatic repulsion through coating with a copolymer. Further endowment of this multifunctional drug delivery platform with targeting ligands and nanovalves may further enhance cell-specific targeting and on-demand release.

KEYWORDS: mesoporous silica nanoparticles · enhanced permeability and retention effect · nanocarrier · cancer treatment · doxorubicin · optimal design · monodisperse · polyethyleneimine–polyethylene glycol copolymer

Mesoporous silica nanoparticles (MSNP) is a multifunctional delivery platform that has been shown at cellular and *in vivo* levels to be capable of delivering chemotherapeutic agents and DNA/siRNA to a variety of cancer cell types.[1–9] This delivery platform allows effective and protective packaging of hydrophobic and charged anticancer drugs for controlled and on demand delivery, with the additional capability to also image the delivery site.[4] The key challenge now is to optimize the design features for efficient and safe *in vivo* drug delivery,[2,10–12] which will be assessed through the use of human xenograft tumors in nude mice.[13]

While the availability of nanocarrier drug delivery systems is an exciting development that holds the promise of a fundamental change in cancer chemotherapy, we are still at a relatively early stage of the implementation of this technology that often contains overblown claims of drug delivery nanoparticles acting as magic bullets. Such claims include the putative ability of active tumor targeting with the ability of selectively sparing all normal tissues. However, the reality is that most nanocarriers are particulates that are recognized by and are effectively removed by the mononuclear phagocytic cells in the reticuloendothelial system (RES) of the liver and spleen.[14] This sequestration is often enhanced by the surface coating of nanoparticles with a corona of proteins that lead to opsonization and enhance phagocytosis by the RES.[15] Moreover, there is also a possibility that the encapsulated drugs could be lost from the carrier or degraded, as well as the fact that the colloidal instability of the carrier could lead to agglomeration in the circulation and may therefore be excluded from the intended "target site". It is also possible that the

* Address correspondence to Anel@mednet.ucla.edu, Zink@chem.ucla.edu.

Received for review February 28, 2011 and accepted April 15, 2011.

Published online April 27, 2011
10.1021/nn200809t

nanocarrier may reach the target site but that the drug is not released from the particle or that the carrier is not taken up effectively in the tumor cells. Both effects will lead to insufficient intracellular drug delivery. Finally, there is also the concern that the heterogeneity among different tumor types could lead to considerable variation in the magnitude of the enhanced permeability and retention (EPR) effect due to differences in vascularity or lymphatic drainage.[16] Given these constraints, it is not a surprise that drug delivery to the tumor site seldom achieves more than 10% of the total administered dose. In fact, few publications show the actual calculation of the EPR effect of the nanocarriers being described.[17]

There are a number of nanomaterial design options for improving the pharmacokinetics, biodistribution, and delivery of anticancer drugs to the tumor site.[18−20] The EPR effect is due to a combination of the abnormally large fenestrations of tumor vasculature and the inefficient lymphatic drainage, which generates the retention effect.[21−23] A preliminary study using our first-generation MSNP that has a ~100 nm primary particle size has shown that these particles could be taken up and accumulate in a human breast cancer (MCF-7) xenograft in nude mice.[13] However, we did not calculate the EPR effect in this study and have since come to realize that the original synthesis method yields particles that agglomerate extensively in biological media. Aggregation could reduce the effectiveness of our original design from an EPR perspective insofar as the preferred particle size is generally considered to be in the 50−100 nm size range.[19,24,25] Thus, size reduction could be helpful to increase the passive targeting effects of our MSNP but also has to consider that even if the size was shrunken, the ionic conditions and proteins present in biological fluids could contribute to agglomeration and that this may require additional design features.[19] A frequent strategy that is being used is to decorate the particle surface with polyethylene glycol (PEG) to provide steric hindrance to improve particle dispersion. Because this feature also leads to interference in particle opsonization, there is a concomitant increase in circulatory half-life as well as an improvement in the EPR effect.[2,21,26] The potential downside of surface coating is that PEG may also interfere in particle uptake by the tumor cells and that the longer circulation time may increase drug leakage from the carrier. In addition to steric hindrance, the addition of a cationic charge to the PEG by using a polyethyleneimine−polyethylene glycol (PEI-PEG) copolymer can further improve particle dispersal due to electrostatic repulsion while also helping to maintain an effective size.

In this study we use a dynamic design strategy to improve the biodistribution and the EPR effect of the first-generation MSNP to improve doxorubicin delivery to a human squamous carcinoma xenograft in nude mice. We demonstrate a dramatic improvement of the EPR effect by reducing the primary particle size to ~50 nm[14] as well as by decorating the particle surface with a PEI-PEG copolymer. We show that these design features in combination with the electrostatic binding of doxorubicin to phosphonate groups in the particle pore allow efficient doxorubicin delivery, some due to intracellular release, at the cancer site.[5] Not only are these design features superior to induce tumor shrinkage and apoptosis compared to the free drug, but also dramatically improve the safety profile of systemic doxorubicin delivery.

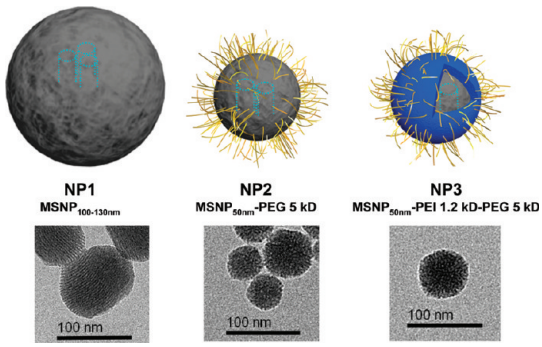

Figure 1. Graphical representation of the MSNP design. NP1 refers to the first-generation phosphonate-coated MSNP with a primary particle size of 100 nm. NP2 was PEGylated with a mesoporous silica core size of 50 nm and coated with a 5 kD PEG polymer. NP3 represents the same core size as NP2, but was coated with a 1.2 kD PEI polymer in which some of the amines were reacted with 5 kD PEG. The pore diameter of all three generations of particles was 2.5 nm. The TEM images at the bottom demonstrate the primary particle size and ordered pore structure.

RESULTS

Synthesis and Physicochemical Characterization of MSNP. In order to achieve an optimal MSNP delivery system for doxorubicin carriage to a human squamous carcinoma xenograft in nude mice, three generations of particles (designated NP1-NP3) were developed (Figure 1). NP1 denotes the first generation of a phosphonate-coated MSNP with a primary size of ~100 nm and exhibiting a negative zeta potential (Figure 2A). We have shown that these particles are useful for the electrostatic attachment and proton-dependent doxorubicin release in acidifying endosomal compartments in cancer cells.[4−7] NP1 is also capable of delivering camptothecin to a human breast cancer (MCF-7) xenograft.[13] However, because of this particle's relatively large primary size and high rate of agglomeration in saline (Figure 2A and B) and other biological media (*e.g.*, 306 nm in DMEM medium; 867 nm in BEGM medium),[7] it was necessary to consider reducing its size as well as changing its surface characteristics to improve the EPR effect. The first approach was synthesis of NP2 (Figure 1), which exhibits a primary size of 50 nm (as determined by TEM analysis) before undergoing PEGylation. Following its coating with a 5 kD PEG polymer, NP2 exhibits a hydrodynamic diameter of ~70 nm, as determined by DLS (Figures 1 and 2). However, while this particle exhibits a negative zeta potential and a hydrodynamic size of 70 nm in water

A

Particle type	Primary size (nm)	Size in H_2O (nm)	Size in Saline (nm)	Zeta Potential in H_2O (mV)
NP1	100	260	520	-25.0
NP2	50	70	597	-20.5
NP3	50	77	110	+46.7

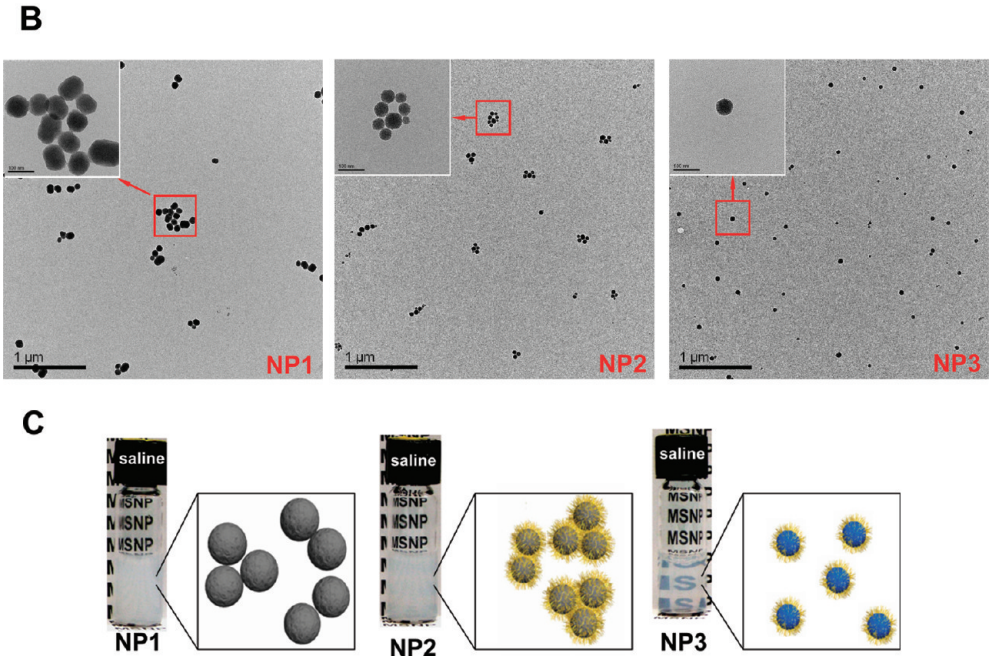

Figure 2. Physicochemical characterization of the different MSNPs. (A) Particle size and zeta potential in pure water and saline were assessed with a ZetaSizer Nano (Malvern), with the particle concentrations at 100 μg/mL. Note that the size and zeta potential were not significantly changed before and after doxorubicin loading (not shown). (B) TEM images demonstrating particle size and dispersal in saline. (C) Photographs of the particles suspended in saline at 20 mg/mL against an appropriate background were taken and supplemented with the illustrations to show that NP3 coated with PEI-PEG had optical transparency because of electrostatic monodispersion, while the other particle types agglomerated for reasons discussed in the text.

(Figure 2A), it undergoes considerable agglomeration in saline with potential interference in extravasation at the tumor site. It was therefore necessary to construct a 50 nm primary particle (Figure 1) coated with a PEI-PEG copolymer to take advantage of the stronger electrostatic repulsion of a cationic particle surface. This yielded a particle with a positive zeta potential, hydrodynamic diameter of ~77 nm in water, and a size of 110 nm in saline (Figure 2A). The improved dispersal of NP3 was confirmed by TEM, showing that NP3 is essentially monodispersed in saline, while NP2 and NP1 form incrementally larger agglomerates (Figure 2B). To further illustrate the dispersal characteristics of the saline-suspended particles, photographic images were obtained and showed optical transparency of the NP3 suspension, while the previous particle generations resulted in turbid suspensions (Figure 2C).

Comparison of the Biodistribution of Labeled and Drug-Laden NP1-NP3 *in Vivo*. In order to determine whether the redesign of particle size and surface coating improve the biodistribution of the various MSNP types, imaging studies were performed in a nude mouse model used for subcutaneous growth of a human tumor xenograft. To visualize the tumor growth in a doxorubicin-sensitive HeLa squamous carcinoma cell line, KB-31 cells were used for stable transfection with a luciferase vector and then used for obtaining bioluminescence images in the mice following intraperitoneal (i.p.) injection of D-Luciferin (Figure 3A, first row). To also visualize the particles *in vivo*, the MSNPs were designed to incorporate a near-infrared (NIR) dye that exhibits high photon penetration in the animal tissue.[27,28] In order to quantitatively compare the biodistribution of NP1–NP3, we showed that the particles had similar labeling efficiency per unit mass (Supporting Information, Figure S1). Initial reference images were obtained prior to particle injection to show a very low NIR background in the tumor-bearing animals (Figure 3A, second row). These animals were then injected with 50 mg/kg of each NIR dye-labeled particle types *via* the tail vein and fluorescence images were captured at the indicated time points (Figure 3A, third–fifth row). The supine images indicate that the majority of NP1 was captured by the liver and spleen

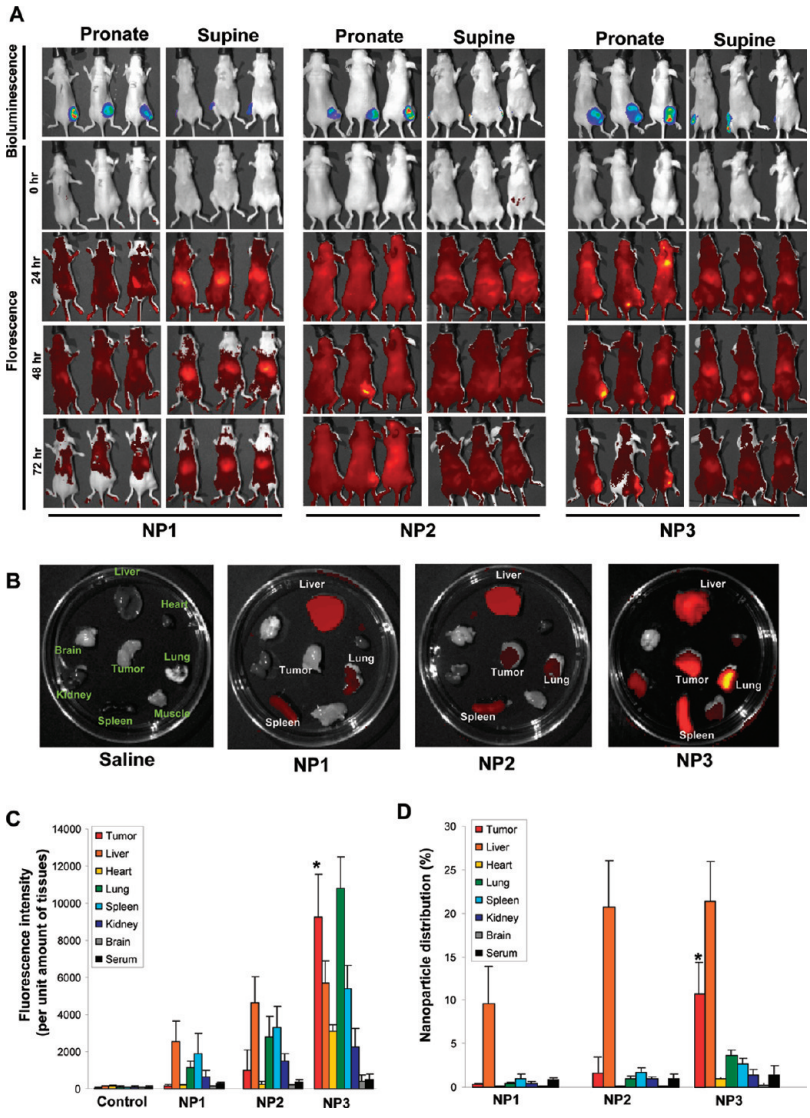

Figure 3. Biodistribution of NIR dye-labeled MSNP to the KB-31-luc tumor xenograft model in nude mice. Particle labeling was performed with Dylight 680 dye as described in Materials and Methods. (A) An IVIS optical imaging system (Xenogen) was used to study the biodistribution of NIR dye labeled MSNP in the tumor-bearing mice. To visualize the luciferase expression in the KB-31 cells, anesthetized mice received intraperitoneal injection of 75 mg/kg D-Luciferin, followed 8 min later by obtaining the bioluminescence images using 10 s exposure time. Reference fluorescence images were captured before intravenous injection of 50 mg/kg NIR-labeled particles into the tumor-bearing mice. Pronate and supine images were obtained at the indicated time intervals following the particle injection. (B) 72 h after injection, the animals were sacrificed and tumor tissues as well as major organs (heart, lung, spleen, liver, kidney, brain, and muscle) were collected for *ex vivo* imaging. (C) Measurement of the fluorescence intensities of individual organs from mice treated with each particle type. Around ~100 mg of tissue for each organ was accurately weighted and homogenized, and the fluorescence intensity obtained at excitation and emission wavelengths of 680/715 nm in a microplate reader (SpectraMax M5e, Molecular Devices, USA). The data represent the mean fluorescence intensity of 1 mg of tissue from the tumor or each organ. *$p < 0.05$, compared with NP1 and NP2. (D) The biodistribution of each particle type was expressed as percent of total load of each nanoparticle distributing to the individual organs. This percent is determined according to the formula [(tissue fluorescent intensity per mg mass tissue × tissue weight in mg)/(total injected particle fluorescent intensity)] × 100%. NP3 yielded a passive tumor accumulation of ~12% of the injected dose, which is significantly higher compared to the treatments using NP1 and NP2. *$p < 0.05$, compared to NP1 and NP2.

within 24 h, and this profiling was maintained for at least 72 h. By contrast, NP2 showed less prominent liver uptake, with a sustained systemic distribution (longer circulation time), indicating the ability of PEG coating to decrease particle opsonization and removal by the RES. Interestingly, a barely visible tumor signal could be obtained in only one of three animals (Figure 3A, middle panel). A similar reduction in RES uptake and increased circulation time were obtained for NP3, which showed prominent particle uptake in the tumor tissue at 24 h, suggestive of a strong EPR effect (Figure 3A, right panel). Moreover, the fluorescence intensity at the tumor site increased gradually, peaking at 48 h, and was then sustained for at least 72 h.

In order to obtain more quantitative data that can be used for calculating the EPR effect, the same

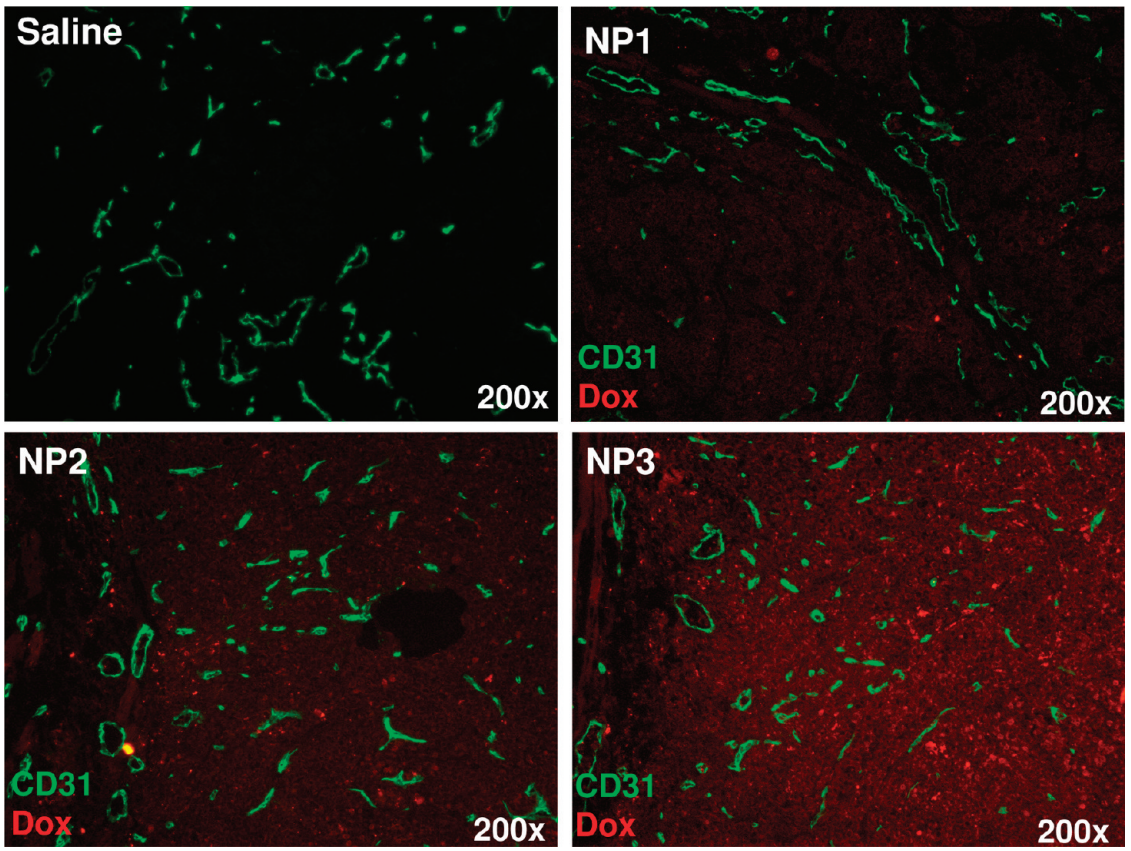

Figure 4. Dual color fluorescence to show the tumor localization of the doxorubicin in relation to the tumor blood vessels detected by a CD31 biomarker. Tumor-bearing mice received intravenous administration of doxorubicin-loaded particles, each at a dose of 50 mg/kg for 72 h. Tumor tissues were collected immediately following animal sacrifice. Histological staining of the OCT embedded frozen tumor tissues in each group was performed by the UCLA Division of Laboratory Animal Medicine (DLAM) diagnostic laboratory services. The sections were incubated with a CD31 primary antibody and visualized by FITC-conjugated secondary antibody. The red fluorescence of doxorubicin was also captured for the same slide view, and merged images were prepared to show intratumoral distribution of the drug in relation to the blood vessels. Slides were visualized under a fluorescence microscope (Zeiss, Germany). It is possible to discern some speckled fluorescence in the lower panels, suggesting that some of the drug is still encapsulated in the particles.

animals were sacrificed at 72 h postinjection, and *ex vivo* fluorescence intensity images were obtained for the tumor tissue as well as major organs such as liver, spleen, lung, kidney, brain, muscle, and heart (Figure 3B). Consistent with the *in vivo* images, NP3 showed the highest fluorescence intensity in the tumor tissue compared to other particle types (Figure 3B). However, NP3 showed abundant distribution to the liver and spleen as well as relatively high fluorescence intensity in the lung compared to the other particle types. The collected organs were accurately weighed and used for the quantitative analysis of particle distribution by expressing the fluorescence intensity per unit mass of tissue (Figure 3C). This readout demonstrated the highest particle concentration at the tumor site in animals treated with NP3 (Figure 3C). When expressed as a percentage of the total mass of the particles administered, ~1%, ~3%, and ~12% of NP1, NP2, and NP3 load, respectively could be seen to biodistribute to the tumor tissue at 72 h (Figure 3D). To further confirm the EPR calculation based on fluorescence intensity, inductively coupled plasma mass spectrometry (ICP-MS) was used to quantify the Si abundance in the major target organs (tumor, liver, kidney, and spleen) of saline- and NP3-treated animals (Figure S2). Consistent with the fluorescence data, ~10% of the total administered elemental Si dose could be demonstrated in the NP3-treated tumor tissue (Supporting Information, Figure S2). While slightly lower than the estimation of the EPR effect by using fluorescence intensity, it has to be considered that some degree of heterogeneity in tumor vascularity can influence fluorescent imaging intensity to explain this small difference.[29] All considered, the estimated EPR of ~12% in the KB-31 model is exceptionally good compared to other polymer/copolymer-based drug and siRNA nanocarrier delivery platforms, where a passive targeting rate of 3.5−10% has been reported for different particle types.[17,30−32]

In order to determine whether drug loading exerts an effect on particle biodistribution, doxorubicin was loaded into NP1, NP2, and NP3 at w/w ratios of 3.3%, 2.5%, and 3%, respectively. The red fluorescence properties of doxorubicin allowed us to make semiquantitative visual comparisons of the amount of drug in the

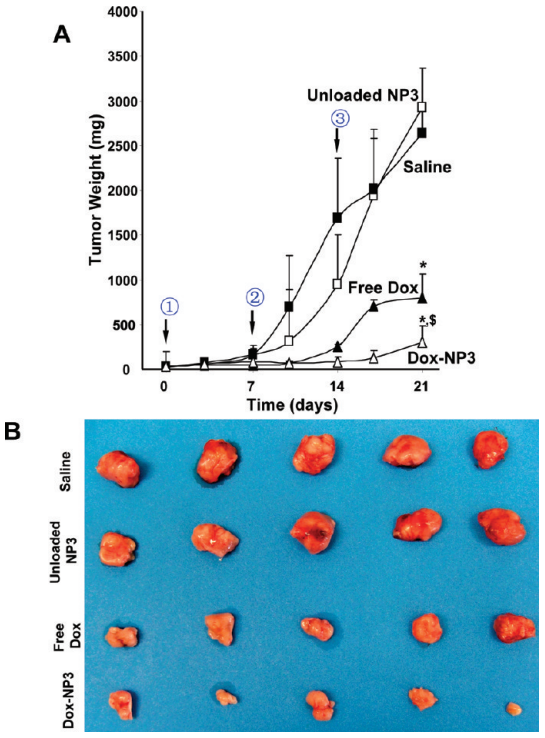

Figure 5. Tumor growth inhibition of doxorubicin-loaded NP3 in tumor-bearing nude mice. (A) Comparison of the tumor inhibition effect of doxorubicin-loaded NP3 (Dox-NP3) *versus* free drug (free Dox), empty particles, and saline in the KB-31 xenograft model. The tumor-bearing mice were intravenously injected with 120 mg/kg doxorubicin-loaded NP3 weekly for 3 weeks. This particle dose is equivalent to 4 mg/kg doxorubicin being delivered to each animal. The animals receiving the free drug were injected with the same amount of doxorubicin weekly for 3 weeks. To compare the effect of NP3 alone, empty particles were intravenously injected at 120 mg/kg, weekly for 3 weeks. The saline group received intravenous saline administration at the same time points. Tumor size was accurately measured twice a week by the same observer. Tumor weight was calculated according to the formula Tumor weight (mg) = (length in mm) × (width in mm)^2/2. *$p < 0.05$, compared to saline; $^{\$}p < 0.05$, compared to free doxorubicin. (B) At the end of this experiment, tumor tissue was collected from each sacrificed animal, and a photograph of the tumor tissue was obtained.

tumor tissue. In order to facilitate this interpretation, the tumor blood vessels were visualized by CD31 immunohistochemistry (Figure 4). This allowed us to visually compare the relative abundance of the drug fluorescence signal in relation to its intratumoral distribution. This analysis showed that doxorubicin delivery by NP3 was the most effective for this type of tumor, and this particle generation was chosen for subsequent studies to perform intravenous drug delivery in the xenograft model as well as for safety assessment compared to treatment with free doxorubicin.

Doxorubicin Delivery and Release by NP3 at the Tumor Site Leads to Efficient Apoptosis and Tumor Shrinkage. Since NP3 exhibits the best EPR effect and is responsible for the highest doxorubicin accumulation in the tumor site, we asked how drug-laden particles compared to free doxorubicin or empty particles in terms of their ability to induce apoptosis and inhibit tumor growth in the KB-31 tumor model. Tumor-bearing animals were injected intravenously on a weekly basis for 3 weeks with a NP3 dose of 120 mg/kg. This is equivalent to the administration of 4 mg/kg doxorubicin per injection and was compared to delivering the same dose of free doxorubicin, injected weekly for 3 weeks. We also included a saline-treated control as well as a group of animals treated with empty particles. When comparing the effect on tumor size, doxorubicin loaded NP3 showed a significantly higher rate of tumor shrinkage than the free drug (Figures 5A and S3). No tumor inhibition was found with saline treatment or the use of empty particles (Figures 5A and S3). Following sacrifice of the animals, the tumor tissues were collected for accurate weighing (Figures 5B and S3). This demonstrated 85% tumor inhibition by doxorubicin-loaded NP3 compared to 70% inhibition by the free drug (Figure 5B). This difference is statistically significant ($p < 0.05$).

Since doxorubicin inhibits cancer cell growth through induction of apoptosis,[33] TUNEL staining was used to compare the abundance and localization of TUNEL-positive cells (green fluorescence) in relation to the doxorubicin fluorescence (Figure 6A). This analysis also allowed us to detect the drug-laden particles in relation to the cells undergoing apoptosis. By merging the red and green fluorescent images, we were able to show from the yellow composites that there is indeed an overlap between the drug and apoptotic cells (Figure 6A, bottom panel). By contrast, the tissues from animals treated with free doxorubicin showed significantly less drug signal, fewer apoptotic cells, and less fluorescence overlap (Figure 6A, left panel). Quantification of the number of TUNEL-positive cells was significantly higher during NP3 delivery of doxorubicin (~38%) compared to mice treated with free drug alone (~13%) (Figure 6B). Additional nuclear staining with Hoechst dye as well as image enlargement of regions "I" and "II" in Figure 6A further demonstrated that the doxorubicin-laden particles could be visualized as red fluorescent specks or dots, frequently appearing in a perinuclear arrangement (Figure 6C, lower panel). This is in favor of cellular entrance of the particles, with presumably some of the drug release taking place in the acidifying endosomal compartment as previously demonstrated by us in KB-31 cells.[6] This stands in contrast to the dull homogeneous background in cancer cells of the mice treated with the free drug (Figure 6C, upper panel).

Doxorubicin Delivery by NP3 Reduces Systemic, Hepatic, and Renal Toxicity Compared to Free Drug. The safety of MSNP drug delivery is of key importance in the assessment of this delivery platform. This includes the inherent safety of the delivery vehicle as well as any potential benefits that may accrue from encapsulated drug delivery. Accordingly, we performed safety profiling by comparing the effects of saline, free

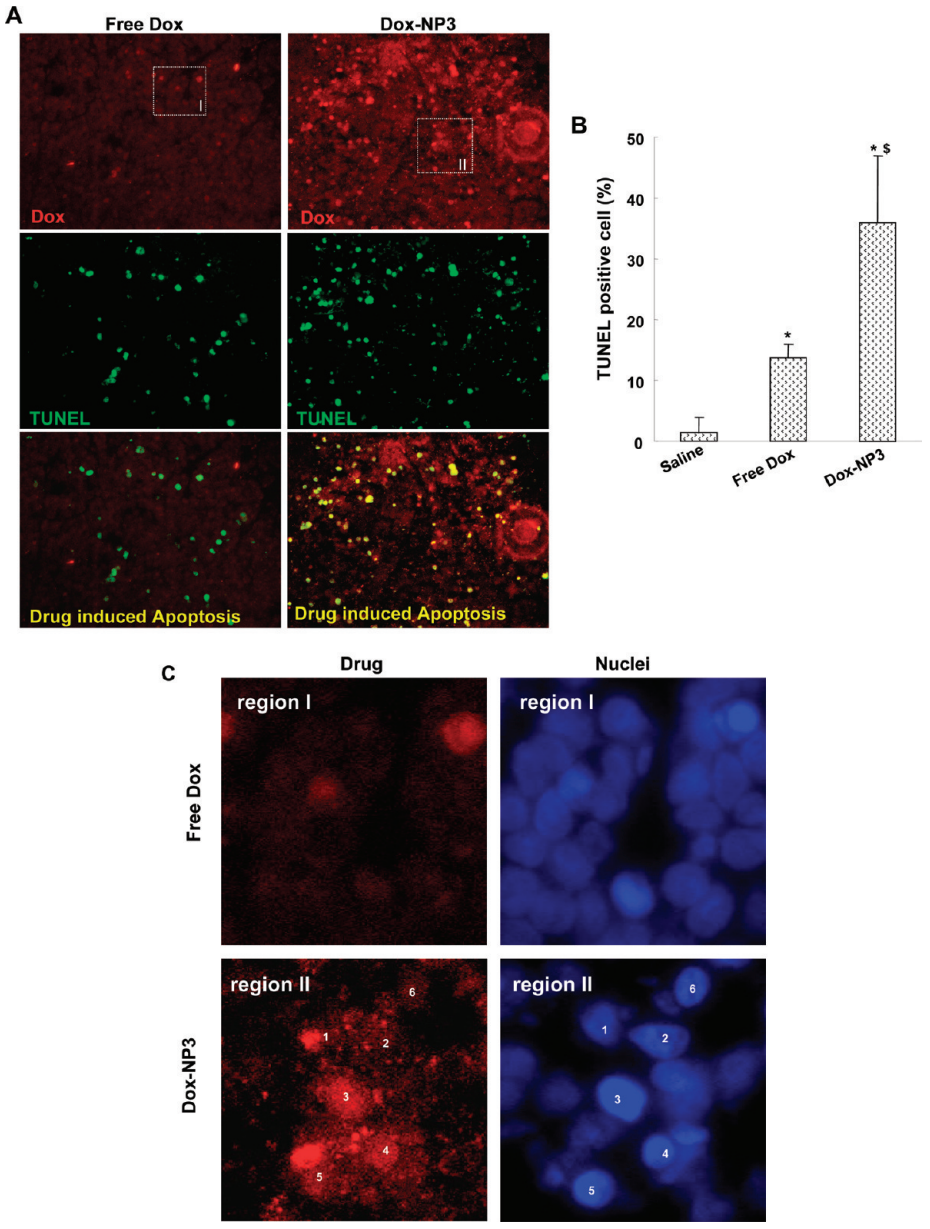

Figure 6. TUNEL staining assay showing enhanced apoptosis and cell death by doxorubicin-loaded NP3 (Dox-NP3) compared to the free drug. (A) To view doxorubicin-induced apoptosis in the tumor tissue, tumor sections were used for TUNEL staining and visualized under a fluorescence microscope. Briefly, a TUNEL detection kit (Invitrogen) was used according to the manufacturer's instructions. Slides of the tumors were washed, fixed, and permeabilized before TUNEL staining. The number of TUNEL positive cells (in green) was scored under the fluorescence microscope (200×). Utilizing its red fluorescence properties, we could also capture the doxorubicin signal in the same tumor section. After merging of the images, the composite yellow spots suggest the presence of delivered drug inside the apoptotic cells. Higher magnification images, including Hoechst nuclear staining of regions "I" and "II", were obtained to further distinguish between free drug and NP3-encapsulated doxorubicin (see panel C). (B) Quantitative analysis of TUNEL-positive cells for each treatment. At least three fields were counted by the same investigator to calculate the percentage of TUNEL-positive cells. *$p < 0.05$, compared to free doxorubicin. (C) Higher magnification images of regions "I" and "II" representing free or Dox-NP3-treated animals. Hoechst dye staining was used to demonstrate the localization of the red fluorescent specks in relation to the nucleus (as indicated by number). In contrast, the free drug yielded more diffuse and dull fluorescence, suggesting that the specks may indeed represent particles, some being displayed in a perinuclear distribution. This is indicative of particle uptake in the tumor cells.

doxorubicin, empty NP3, and doxorubicin-laden NP3. The safety profiling included assessment of total body weight, blood chemistry, histological examination of major organs, and performance of a red blood cell lysis assay. Compared to saline-treated tumor-bearing mice, no significant body weight changes were observed during the administration of either empty NP3 or nanoparticles loaded with doxorubicin (Figure 7A). In contrast, animals receiving free doxorubicin administration showed a cyclical decrease in body weight following each of the weekly drug administrations (Figure 7A). Moreover, these animals also showed

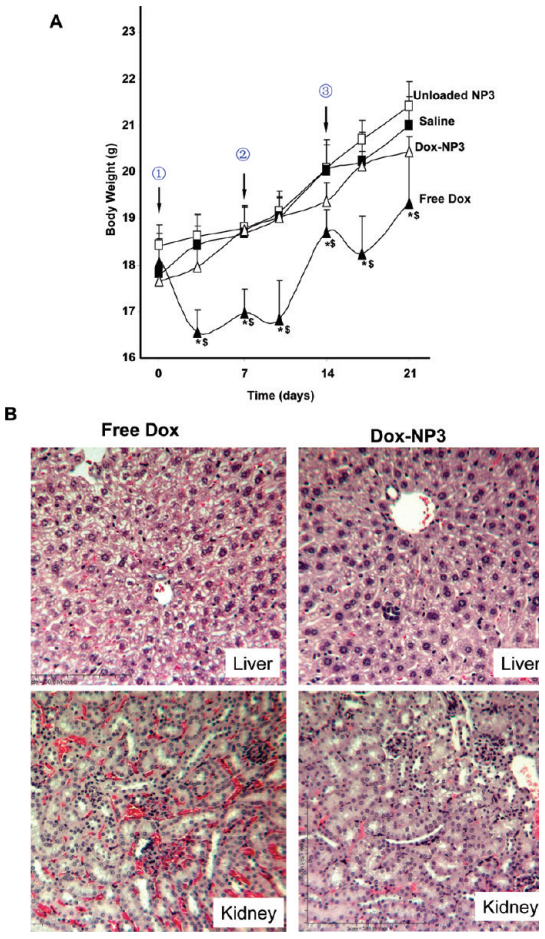

Figure 7. Assessment of treatment on animal weight as well as liver and kidney histology. (A) The animal weights were recorded twice a week and expressed for the three-week experimental duration. (B) Histological analyses of liver and kidney sections were performed by UCLA DLAM diagnostic laboratory services. The sections were stained with hematoxylin/eosin (H&E) and examined by light microscopy. Representative images are shown. The hepatic histology reveals steatosis of the liver in the free doxorubicin-treated group. In contrast, the liver histology was normal for animals treated with the same amount of drug encapsulated in NP3. The liver histology of animals receiving empty NP3 or saline was also documented as normal (see Supporting Information, Figure S4). The kidney histology demonstrates the generation of glomerular swelling and nephrotoxicity by free doxorubicin, while animals treated with the encapsulated drug had no histological abnormalities. The histology was also reported as normal in animals receiving empty NP3 or saline (see Supporting Information, Figure S4).

significant elevations of the liver function enzymes alanine aminotransferase (ALT) and aspartate aminotransferase (AST), as well as an increased total bilirubin (TBIL) value compared to the saline control (Table 1). In addition, the doxorubicin-treated animals showed a mild increase in inorganic phosphate (PHOS) levels (Table 1). In contrast, when doxorubicin was delivered by NP3, the ALT, PHOS, and TBIL levels stayed normal with only a smaller but significant increase in the AST level (Table 1). In mice treated with the empty NP3 carrier, biochemical analysis did not show any significant changes in liver function, kidney function (blood urea nitrogen, BUN; creatinine, CRE), cholesterol (CHOL), triglycerides (TRG), glucose (GLU), PHOS, total protein (TPR), calcium (CAL), and albumin (ALB) (Table 1).

TABLE 1. Serum Biochemistry Profiles

biochemical parameter[a]	saline	unloaded NP3	free Dox	Dox-NP3
CHOL (mg/dL)	110.0 ± 18.2	118.0 ± 18.4	97.8 ± 12.8	122.3 ± 8.5
TRG (mg/dL)	79.0 ± 36.5	110.3 ± 22.5	91.5 ± 21.2	96.0 ± 24.9
ALT (u/L)	23.3 ± 6.8	26.7 ± 4.0	36.8 ± 8.0[b]	27.3 ± 2.1[c]
AST (u/L)	132.0 ± 23.4	183.3 ± 23.2	347.8 ± 73.9[b]	174.0 ± 38.2[c]
TBIL (mg/dL)	0.2 ± 0.0	0.3 ± 0.0	0.4 ± 0.0[b]	0.2 ± 0.0[c]
GLU (mg/dL)	111.3 ± 18.6	106.0 ± 20.4	102.5 ± 29.2	108.0 ± 9.4
PHOS (mg/dL)	8.6 ± 0.7	8.5 ± 0.2	9.5 ± 0.8[b]	7.5 ± 0.7[c]
TPR (g/dL)	4.8 ± 0.3	5.7 ± 0.2	5.0 ± 0.4	5.4 ± 0.2
CAL (mg/dL)	9.4 ± 0.2	9.7 ± 0.2	9.0 ± 0.5	9.8 ± 0.1
BUN (mg/dL)	16.0 ± 2.6	20.0 ± 4.4	17.3 ± 2.6	19.0 ± 4.1
CRE (mg/dL)	0.3 ± 0.0	0.3 ± 0.0	0.3 ± 0.1	0.3 ± 0.0
ALB (g/dL)	2.3 ± 0.2	2.8 ± 0.1	2.4 ± 0.2	2.6 ± 0.1

[a] Blood was collected from the sacrificed animals, and the serum obtained by centrifuging the whole blood at 5000 rpm for 15 min. The biochemical parameters were assayed by UCLA Division of Laboratory Animal Medicine (DLAM) diagnostic laboratory services. These parameters include cholesterol (CHOL), triglycerides (TRG), alanine aminotransferase (ALT), aspartate aminotransferase (AST), total bilirubin (TBILI), glucose (GLU), inorganic phosphorus (PHOS), total protein (TPR), calcium (CAL), blood urea nitrogen (BUN), creatinine (CRE), and albumin (ALB). [b] $p < 0.05$, compared to saline. [c] $p < 0.05$, compared to free doxorubicin.

Histological examination of the liver showed prominent hepatic steatosis in the animals treated with free doxorubicin (Figure 7B, upper panel).[34] Steatosis represents fatty degeneration as a result of metabolic impairment of triglyceride synthesis and elimination and is a frequent feature of toxic liver injury, including during chemotherapy.[35,36] No steatosis was observed in any of the other treatment groups (Supporting Information, Figure S4, upper panel). Free doxorubicin delivery also resulted in nephrotoxicity, which manifested as glomerular swelling (Figure 7B, lower panel).[37] No significant abnormalities were found in the mice treated by saline or empty particle (Supporting Information, Figure S4, lower panel). Since the NP3 also abundantly biodistributed in lung, histological examination of the lung tissue was performed but did not show any gross pathology resulting from empty or drug-loaded NP3 (Supporting Information, Figure S5). Interestingly, histological examination of myocardial tissue did not show any gross pathology in any of the experimental groups (Supporting Information, Figure S6). This is probably due to the relatively low doxorubicin dose and short treatment period in our study.[38]

Because the cationic (PEI) component of our copolymer coating is potentially toxic to cell membranes, including the ability to lyse red blood cells (RBC), we performed a hemolysis assay using heparinized mouse RBC.[39] The results did not show any hemoglobin release in response to empty NP3 at concentrations as high as

2500 μg/mL (Supporting Information, Figure S7). This is at least 10 times higher than the therapeutic dose requirements. These results are in agreement with our previous study showing that coating of the MSNP surface with shorter length (<10 KD) PEI polymers do not lead to significant toxicity in a range of normal and tumor cells.[7]

DISCUSSION

By using size tuning and decoration of the MSNP surface with a PEI-PEG copolymer, we were able to improve particle dispersal and biodistribution to achieve therapeutically useful doxorubicin delivery to a tumor xenograft site in nude mice. Through the use of NIR fluorescence imaging and elemental Si analysis, we showed that a 50 nm particle consisting of a mesoporous silica core coated with the PEI-PEG copolymer was capable of achieving an excellent EPR effect compared to noncoated larger particles (NP1) or a 50 nm particle decorated with PEG only (NP2). In addition to passive particle accumulation at the tumor site, NP3 was also capable of entering KB-31 tumor cells to deliver a toxic dose of doxorubicin and inducing a higher rate of apoptosis compared to the free drug. The encapsulated drug was also associated with less systemic, hepatic, and renal toxicity compared to free doxorubicin. This is the first demonstration of how the optimal design of the MSNP platform can achieve passive drug delivery, which in combination with intracellular uptake resulted in an efficacious antitumor effect.

While each of our design features are recognized modifications for improving the therapeutic efficacy of nanomaterials, their integrated use through a series of design improvements to achieve *in vivo* tumor shrinkage and EPR > 10% has not been described previously for MSNPs. The best recorded EPR effects with a polymer- or copolymer-based nanocarrier system with therapeutic efficacy were in the range 3.5% to 10%.[17,40,41] Our ability to exceed this delivery with our MSNP platform is highly significant since this has been achieved without targeting ligands or the use of sophisticated design features such as the attachment of nanovalves.[1,4,6] The first step in improving our MSNP design was to construct a 50 nm mesoporous silica core to approach a carrier size more conducive for slipping past the malformed blood vessel fenestrations in the tumor. This feature was achieved by using a co-templating agent method for particle synthesis. This involves addition of an optimal amount of Pluronic F127 to cetyl trimethylammonium bromide (CTAB), which is the standard surfactant used for synthesis of the first-generation MSNP.[4−7] The Pluronic F127 changes the structure of the CTAB micelles, which affects their micelle packing behavior, therefore leading to a smaller particle size.[42] Pluronic F127 also improves the dispersion of the hydrophobic silica precursor, tetraorthoethylsilicate (TEOS), and also coats newly formed MSNPs, helping to protect them from agglomeration and oligomerization.

The second key design feature is PEGylation of the MSNP surface, which results in reduced RES uptake, as demonstrated for NP2 and NP3. This prolongs the particles' circulation time, which has a direct bearing on the EPR effect. Similar to our findings, He *et al.* previously demonstrated that PEGylation of an 80 nm MSNP results in a longer blood-circulation lifetime compared to naked particles in healthy ICR mice.[2] However, in our study PEGylation alone achieved an EPR effect of only ~3% for NP2, because the particles agglomerated to ~600 nm size, thereby preventing extravasation the tumor site. Although PEG provides steric hindrance that could theoretically interfere in nanoparticle aggregation in water, the increased ionic strength of biological media compresses the electric double layer on the particle surface.[43−45] This significantly weakens the repulsion between particles. The introduction of cationic charge by using a PEI copolymer overcame this problem. It is also important to mention that reduced particle opsonization after PEGylation may also reduce immunogenic potential, thereby adding an additional safe design feature.[7]

The attachment of the PEI-PEG copolymer was undertaken with a view of improving the MSNP dispersal and thereby reducing the particle's hydrodynamic size to be as close as possible to the primary particle size. The effectiveness of the strategy was demonstrated by the acquisition of a positive zeta potential on NP3 as well as achieving a monodisperse suspension with an average hydrodynamic size of ~100 nm in saline. Similar use of a copolymer strategy to shrink particle size to improve dispersal was previously demonstrated in the preparation of albumin nanoparticles,[46] PEI-PEG block copolymer,[43−45] gold nanoparticles,[47] and silica particles.[48] In particular, the use of a PEI-PEG copolymer resulted in the smallest possible hydrodynamic size and the best state of dispersal of these materials compared to coating with PEG only. To illustrate the importance of the cationic charge in achieving these design features, we neutralized the amine groups on the PEI in the copolymer with phthalic anhydride and could demonstrate that the less cationic NP3 underwent a dramatic size increase in saline (Supporting Information, Figure S8). Consistent with the previous research using trimethylammonium-modified MSNP with a primary size of 50−100 nm capable of liver accumulation,[3] it would appear that the size reduction effect of the PEI-PEG coating is the major reason for improving biodistribution and therapeutic outcome. While not pursued in this article, the placement of a positive charge on the MSNP surface endows these particles with the ability to bind, protect, and deliver nucleic acids. We have recently demonstrated that PEI coating of the first-generation MSNP is useful for the delivery of a P-glycoprotein (Pgp) siRNA that restores doxorubicin

sensitivity in a doxorubicin-resistant HeLa cell line.[5] Similar *in vivo* studies are being contemplated for the future.

The EPR effect of therapeutic nanoparticles plays a key role in their accumulation at the tumor site. Compared to nanoparticles containing surface ligands that promote active targeting of tumor cells or tumor tissue, the use of the EPR effect is considered to be a passive targeting strategy.[26,49] Nonetheless, the EPR effect is tunable and can be accomplished through redesign of the nanocarrier or manipulating the tumor microenvironment. Examples of the latter strategy include elevation of systemic blood pressure by angiotensis II,[50] using a vasodilator such as NO-releasing agents,[51] or increasing vascular permeability with biomolecules such as VEGF and iRGD peptide.[52,53] However, all of these adjuvant treatments pose some hazard and may not be useful for every treatment consideration. Redesign of the nanomaterial could also impact the EPR effect as reviewed above. It is important to mention here that after their extravasation the cellular attachment and uptake of the nanoparticles are dependent on their diffusion and that the diffusion constant is inversely correlated to nanoparticle size.[24] In this regard it has previously been shown that the size reduction of block copolymer micelles through a correct combination of polymers could enhance this nanocarrier's uptake in a human breast cancer xenograft.[24] It is further worth noting that the EPR effect is highly dependent on the cancer type, including the extent of neo-angiogenesis and the vascularity of the tumor.[54,55] While in a previous study our first-generation MSNP was capable of accumulating in a human breast carcinoma (MCF-7) xenograft,[13] we could not obtain a satisfactory EPR effect with this material in the KB-31 model. However, we did demonstrate through size reduction as well as coating the 50 nm particles with a PEI-PEG copolymer that we could increase particle uptake by an order of magnitude in KB-31 tumor sites. Moreover, we showed that the passive enhancement of NP3 accumulation at these tumor sites is accompanied by intracellular uptake without requiring the attachment of a ligand. The cationic particle surface could play an active role in promoting this uptake as previously demonstrated in a variety of cancer cell types *in vitro*.[7]

Key to any therapeutic intervention is the inherent safety of the delivery system. We are pleased that the empty NP3 failed to elicit any adverse effects after intravenous injection, as determined by animal body weight, blood biochemistry, and histological analysis of major organs and tissues. Moreover, these particles did not damage red cell membranes when using a hemolysis assay (Supporting Information, Figure S7). Another design feature to consider from a safety perspective is particle coating with a PEI polymer. While it is well known that PEI by itself or coated onto particle surfaces could lead to toxicity, we have previously demonstrated that this toxicity is dependent on the polymer length and cationic charge density.[7] Thus, while high molecular weight (≥10 kD) PEI polymers can induce considerable cellular toxicity in a variety of normal and transformed cell types, there is no generation of cellular toxicity by the 1.2 kD polymer used in this work.[7] This was confirmed by conducting cytotoxicity studies with NP3 in cancer cell lines (not shown). The apparent reason is the distribution and density of cationic charge on the longer length *versus* the shorter length PEI polymers, allowing the longer length polymers to induce membrane damage as well as the possibility of inducing a so-called "proton sponge effect" that is associated with lysosomal damage.[7,56] It is also worth mentioning that intravenous injection of the equivalent of NP1 coated with a 25 kD PEI polymer in mice did not elicit any significant toxicity in a previous study in mice.[7]

Equally important is the demonstration of the improvement of the high level of doxorubicin toxicity by encapsulating the drug in NP3.[57,58] Thus, compared to the free drug, doxorubicin encapsulation did not exert an effect on total body weight or impact liver and kidney function (Figures 7C and S4). Interestingly, we did not observe evidence of histological damage to the myocardium in this study, even with free doxorubicin.[59] This may be due to the comparatively high sensitivity of KB-31 cancer cells to the effects of doxorubicin.[5] This reduction of systemic toxicity is likely due to the drug being bound to the negatively charged phosphonate groups in the particle pores, therefore not being released in the bloodstream. We have previously demonstrated that doxorubicin release from phosphonate-coated MSNP pores takes place in the acidifying endosomal compartment in KB-31 cells.[5] While it is difficult to study endosomal release at the intact animal level, our fluorescence visualization data demonstrate the presence of doxorubicin-containing NP3 in a perinuclear distribution in KB-31 cells undergoing apoptosis *in vivo* (Figure 6C). Thus, we propose that intracellular drug release contributes to the higher rate of KB-31 cell apoptosis in this study. We may be able to further enhance this feature by using a pH-dependent nanovalve that is capable of opening intracellularly in KB-31 cells with the capability of doxorubicin release to the nucleus.[6]

It is important to mention that, similar to other nanocarriers,[60] the vast majority of systemically administered MSNPs are sequestered by the RES irrespective of the design feature. The lack of observable toxicity of the doxorubicin-laden particles in the liver and spleen is an interesting finding that has not been resolved as yet. One possibility is that the traditional biomarkers used for following liver injury are ineffective in reflecting RES damage, but another explanation is that the RES and organs like the liver are quite

resilient in dealing with doxorubicin toxicity when the drug is encapsulated. This could involve protective features such as hepatobiliary transfer, which has been shown to be quite prominent in another MSNP study.[61] It is also possible that the relatively slow rate of drug release from the particle pores could prevent acute toxicity due to drug conjugation, inactivation, or excretion.[21,22] There is also a considerable capacity of mononuclear macrophages to destroy or sequester particulate matter.[62] It is important to mention that in a previous study we have demonstrated that tracking of elemental Si following systemic MSNP administration could lead to the recovery of ~94% of the injected MSNP bolus in the urine and feces within 4 days.[10] This is in agreement with the demonstration by Souris *et al.* of the rapid bioelimination of MSNP through hepatobiliary excretion in murine experiments.[61] This constitutes another important safety feature of a nanocarrier that either could be degraded *in situ* into cellular subcomponents or could be excreted from the body once the carrier has served its therapeutic purpose. The *in vivo* biodegradability and bioelimination of MSNP is comparable to abiotic studies, showing the gradual decomposition of MSNP in simulated body fluids at 37 °C, including demonstrating a breakdown of the MSNP architecture with a decrease in their BET surface area.[63]

CONCLUSION

In this paper, we have demonstrated that size tuning and decoration of the MSNP surface with a PEI-PEG copolymer constitutes an efficient doxorubicin delivery strategy for a human squamous carcinoma xenograft in nude mice. Through *in vivo* imaging and elemental analysis we have demonstrated that these design modifications lead to an excellent EPR effect and sufficient nanocarrier accumulation to achieve tumor cell killing that is more effective than the free drug. We further demonstrate that this delivery minimizes the chemotherapeutic side effects at the intact animal level as well as susceptible organs. These results are encouraging from the perspective of moving the MSNP platform into clinical trials as well as introducing additional design features that will make it possible to perform theranostics as well to obtain on-demand drug release at the tumor site by a series of nanovalves that can be controlled through pH, temperature, photon wavelength, or a magnetic field.

MATERIALS AND METHODS

Materials. Cetyl trimethylammonium bromide (CTAB, 95%), Pluronic F127, tetraorthoethylsilicate (TEOS, 98%) 3-(trihydroxysilyl)propyl methylphosphonate (42% in H_2O), polyethyleneimine (PEI, 1.2 kD), 4-(dimethylamino)pyridine (99%), *N*,*N*′-disuccinimidyl carbonate (95%), poly(ethylene glycol) methyl ether (m-PEG, MW 5 kD), phthalic anhydride (99%), and Polybrene were purchased from Sigma (St. Louis, MO). *N*-(2-Aminoethyl)-3-aminopropyltrimethoxysilane (NAPTS) was purchased from Gelest (Morrisville, PA). Amine-reactive near-infrared Fluor DyLight 680 NHS ester was purchased from Thermo Scientific (Rockford, IL). D-Luciferin was purchased from Xenogen (Alameda, CA). Apoptosis TUNEL detection kit (Click-iT TUNEL kit), bovine serum albumin (BSA), DPBS solution, L-glutamine, penicillin, streptomycin, and DMEM medium were obtained from Invitrogen. Fetal bovine serum (FBS) was purchased from Atlanta Biologicals. Anti-CD31 antibody was purchased from BD Bioscience. All reagents were used without further purification.

Synthesis of NP1. We followed well-established procedures to synthesize the classically designed or first-generation MSNP (NP1).[4−6,13] Briefly, 250 mg of CTAB was dissolved in 120 mL of water, followed by the addition of 875 μL of 2 M NaOH aqueous solution. The solution was heated to and kept at 80 °C for 30 min before 1.25 mL of TEOS was added. The solution went from clear to opaque, which is indicative of a hydrolysis process. After 15 min, 315 μL of trihydroxysilylpropyl methylphosphonate was added. The reaction was kept at 80 °C for another 2 h. The resulting nanoparticles were centrifuged and washed with methanol. In order to remove the CTAB, the as-synthesized particles were suspended in 60 mL of methanol and 2.3 mL of 12 M hydrochloride acid. The solution was refluxed for 10 h, and the MSNPs designated NP1 were collected for centrifugation and further washing with methanol.

Synthesis of NP2. A 200 mg amount of Pluronic F127 was mixed with 250 mg of CTAB and 120 mL of H_2O. The solution was heated to 80 °C and kept for 30 min. A 1 mL portion of TEOS was mixed with 200 μL of NAPTS in 1 mL of ethanol and then added dropwise into the CTAB solution. A 300 μL sample of trihydroxysilylpropyl methylphosphonate was added 20 min later. The solution was filtered through a 0.22 μm polycarbonate syringe filter (Millipore, Billerica, MA), and to remove the CTAB, the filtrate was mixed with 120 mL of methanol and 0.8 g of NH_4NO_3. The solution was heated to 70 °C for 30 min. The particles were collected by centrifugation and washed with methanol. To conduct PEG coating, m-PEG was used because this polymer contains only a single reactive hydroxyl group that can be used for PEI attachment; regular PEG has two reactive ends that may cause particle cross-linking. For the attachment to PEI, the hydroxyl group on m-PEG was replaced with a NHS-ester (referred as activated m-PEG) that is capable of reacting with the PEI amine residues. A 10 mg amount of the as-synthesized MSNP was suspended in 1.5 mL of DMF and mixed with 50 mg of activated m-PEG.[7] The solution was stirred for a further 24 h, and the particles were collected, sequentially washed with DMF and ethanol, and eventually resuspended in water.

Synthesis of NP3. The reduced size silica core was synthesized as described above. To perform PEI coating, 10 mg of as-synthesized small MSNP was suspended in 1 mL of 2.5 mg/mL PEI ethanolic solution. The solution was sonicated and stirred for 30 min. This process was repeated twice to substitute the F127 coating that was previously achieved by attaching PEI to the NP3 surface. The particles were further washed in ethanol to remove excess PEI and trace amount of F127 residue. The PEI-coated particle was subsequently transferred into 1.5 mL of DMF, mixed with 50 mg of activated m-PEG, and stirred for 24 h. The nanoparticles were washed with DMF and ethanol and resuspended in water.

NIR Fluorescent Labeling. The NIR fluorescent dye DyLight 680 NHS ester was used for particle labeling. For NP1, 10 mg of all the particles was suspended in 1 mL of ethanol and mixed with 0.1 mg of the DyLight 680 and 0.5 μL of NAPTS. The reaction was kept under inert atmosphere and stirred at room temperature for 12 h. The resulting particles were centrifuged and washed with H_2O. For NP2 and NP3, 10 mg each were suspended in 1 mL of DMF and mixed with 0.1 mg of DyLight 680. After 12 h, the particles were washed with H_2O.

Physicochemical Characterization. All MSNPs were characterized for size distribution, shape, and surface charge. The shape and

structure were characterized using a transmission electron microscope (JEOL JEM 2010, JEOL USA, Inc., Peabody, MA). TEM samples were prepared by placing a drop of the nanoparticle saline suspension at a concentration of 100 μg/mL onto a 200-mesh copper grid (Electron Microscopy Sciences, Washington, PA) and then drying at room temperature overnight. Primary particle size was measured by random sampling of at least 10 particles that were imaged on a TEM grid. Image J software was used to determine the average MSNP diameter. Particle size and zeta potential in solution were measured by ZetaSizer Nano (Malvern Instruments Ltd., Worcestershire, UK). All of the measurements were performed with the nanoparticles suspended in filtered water or saline at 100 μg/mL nanoparticle concentration. Similar analysis was also performed on the doxorubicin-loaded particles.

Drug Loading and Loading Yield Measurement. A 10 mg sample of various particles was suspended in 0.5 mL of 5 mg/mL doxorubicin aqueous suspension. The solution was stirred for 24 h, and the nanoparticles were collected through centrifugation and carefully washed with H_2O. To measure the loading yields of the various particles, 1 mg of doxorubicin-loaded MSNP was resuspended and sonicated in 1 mL of heated 0.1 M HCl for 15 min. After centrifugation, another 1 mL of fresh HCl aqueous solution was added. This process was repeated at least for five times. The pH of the supernatant was readjusted to 7.0 by 1 M NaOH, and the fluorescence spectrum of doxorubicin was measured at excitation and emission wavelengths of 485/550 nm in a microplate reader (SpectraMax M5 microplate reader, Molecular Devices, USA).

Cell Culture and Luciferase Transfection. KB-31 cancer cells were maintained in 25 cm^2 or 75 cm^2 cell culture flasks in which the cells were passaged at 70−80% confluency every 3 days. The cells were cultured in Dulbecco's modified Eagle medium (DMEM) (Carlsbad, CA) containing 10% FBS, 100 U/mL penicillin, 100 μg/mL streptomycin, and 2 mM L-glutamine (complete medium). To generate a stable cell line constitutively expressing luciferase, 1.5 $\times$ 10^4 KB-31 cells in 40 μL of complete DMEM (supplemented with 10% FBS, 100 U/mL penicillin, 100 μg/mL streptomycin, 2 mM L-glutamine, and 8 μL/mL Polybrene) were transduced with 10 μL of a lentivirus (Cignal Finder Lenti Pathway Reporter Qiagen/SA Biosciences; 1.4 $\times$ 10^7 TU/mL) in 96-well tissue culture plates. Spinoculation (centrifugal inoculation) was performed at 1200*g* for 60 min. The viral-containing media was removed after 16 h, and the cultures were replenished with fresh DMEM media. Cells were allowed to proliferate to a population size of 1.2 $\times$ 10^6 cells. A heterogeneous pool of transduced cells was selected by using 1 μg/mL puromycin for at least 14 days prior to tumor implantation.

Establishment of the KB-31-luc Tumor Xenograft Model. Athymic BALB/c nu/nu female mice (6 weeks) were purchased from the Charles River Laboratory and maintained under pathogen-free conditions. All animal experiments were performed using protocols approved by the UCLA Animal Research Committee. The tumor cell suspension (0.1 mL, 5 $\times$ 10^6 cells/mL) was injected subcutaneously into the mice. To perform imaging, the tumor-bearing animals were used 2.5 weeks after tumor implantation. In the tumor growth inhibition experiments, the nude mice were randomly divided into four groups and received the listed range of treatments, which commenced 1 week after tumor implantation.

Determining MSNP Biodistribution. The tumor-bearing mice were randomly divided into three groups (n = 3). To visualize the tumor, anesthetized mice were i.p. injected with 75 mg/kg D-luciferin. Eight minutes after injection, bioluminescence images were acquired using an IVIS Imaging System (Xenogen). Acquisition time was 10 s. Subsequently, the mice were intravenously administered with NIR dye-labeled NP1, NP2, or NP3 at doses of 50 mg/kg (~1 mg nanoparticles per mouse), and the fluorescence images were taken at indicated time points. Then 72 h after injection, the tumor tissue together with major organs (heart, lung, spleen, liver, kidney, brain, and cardiac muscle) were collected and used for *ex vivo* imaging. Around ~100 mg of tissue for each organ was accurately weighed out, washed, and homogenated, and the fluorescence intensities per unitary amount of each organ were measured by a microplate reader (Molecular Devices, M5e).

Immunohistochemical Staining to Determine CD31 Expression in the Tumor Tissue. The tumor-bearing mice were randomly divided into three groups (n = 3) and intravenously administered with the doxorubicin-loaded NP1, NP2, or NP3 at doses of 50 mg/kg (~1 mg nanoparticles per mouse). The tumor tissues were rapidly collected after 72 h, frozen, and OCT embedded before sectioning to provide 4 μm thick slices. The slices were washed three times in PBS and fixed in cold acetone for 15 min, and the slide was subsequently blocked using 1% normal goat serum at room temperature for 10 min. The sections were overlaid with rat-anti-mouse CD31 monoclonal antibody (1:500) at 4 °C overnight. After removal of the primary antibody and washing in PBS three times, FITC-labeled goat-anti-rat IgG (1:500) was added and incubated for 1 h at room temperature. The slides were visualized under a fluorescence microscope (Zeiss, Germany).

Nude Mouse Studies to Determine the Effect of Doxorubicin-Loaded NP3 on Tumor Shrinkage. One week after tumor implantation, the KB-31 tumor-bearing mice were randomly divided into four groups of five animals each. These groups were used for comparing the effects of saline, empty nanoparticles, free doxorubicin, and doxorubicin-loaded NP3, respectively. The latter group received intravenous administration of 120 mg/kg (~2.4 mg per animal) NP3, which is equivalent to a doxorubicin dose of 4 mg/kg (~0.08 mg per animal), weekly for 3 weeks. The free doxorubicin group received the same drug dose weekly for 3 weeks, while the group receiving empty NP3 was treated with 120 mg/kg on a weekly basis. The fourth group was treated with saline as control. The body weight and tumor size were accurately recorded twice per week. Tumor weight was calculated according to the formula Tumor weight (mg) = (length in mm) $\times$ (width in mm)^2/2.[64]

TUNEL Staining of the Tumor Tissue. A section of the tumor from each animal was used for TUNEL staining. The slides containing the tumor section were washed, fixed, and permeabilized before performance of TUNEL staining according to the manufacturer's instructions (Invitrogen, Carlsbad, CA). Nuclei were stained by Hoechst 33342 dye. The number of TUNEL-positive cells (green staining) was assessed under a fluorescent microscope (200$\times$). The same sections were also used for recording of the red fluorescent images of the doxorubicin that was present in the particles or the tissues. At least three fields were counted by the same investigator to calculate the percentage of TUNEL-positive cells.

Blood Biochemistry to Assess Possible Toxicity. Following the animal experiments described above, the mice were sacrificed on the 21st day and serum was collected by centrifuging the whole blood at 5000 rpm for 15 min. The biochemical parameters, including cholesterol (CHOL), triglycerides (TRG), alanine aminotransferase (ALT), aspartate aminotransferase (AST), total bilirubin (TBILI), glucose (GLU), inorganic phosphorus (PHOS), total protein (TPR), calcium (CAL), blood urea nitrogen (BUN), creatinine (CRE), and albumin (ALB), were assayed by UCLA Division of Laboratory Animal Medicine (DLAM) diagnostic laboratory services.

Tumor and Major Organ Histology. Appropriate size sections of the tumor, liver, kidney, spleen, lung, heart, and brain were fixed in 10% formalin and then embedded into paraffin. Tissue sections of 4 μm thickness were mounted on glass slides by the UCLA Division of Laboratory Animal Medicine (DLAM) diagnostic laboratory services. The sections were stained with hematoxylin-eosin (H&E) and examined by light microscopy. The slides were read by an experienced veterinary pathologist.

Acknowledgment. This study was funded by the U.S. Public Health Service Grant RO1 CA133697 and NIEHS U19 ES019528 (UCLA Center for NanoBiology and Predictive Toxicology). We thank Bryan France in Dr. Ken Bradley's laboratory for providing technical assistance with luciferase transfection of KB-31 cells, and Juyao Dong for assistance with preparation of the PEI-coated particles.

Supporting Information Available: Additional figures, results, and method descriptions as described in the text. This material is available free of charge *via* the Internet at http://pubs.acs.org.

REFERENCES AND NOTES

1. Lu, J.; Liong, M.; Zink, J.; Tamanoi, F. Mesoporous Silica Nanoparticles as a Delivery System for Hydrophobic Anticancer Drugs. *Small* **2007**, *3*, 1341–1346.
2. He, Q.; Zhang, Z.; Gao, F.; Li, Y.; Shi, J. *In vivo* Biodistribution and Urinary Excretion of Mesoporous Silica Nanoparticles: Effects of Particle Size and PEGylation. *Small* **2011**, *7*, 271–280.
3. Lee, C.-H.; Cheng, S.-H.; Wang, Y.-J.; Chen, Y.-C.; Chen, N.-T.; Souris, J.; Chen, C.-T.; Mou, C.-Y.; Yang, C.-S.; Lo, L.-W. Near-Infrared Mesoporous Silica Nanoparticles for Optical Imaging: Characterization and *In Vivo* Biodistribution. *Adv. Funct. Mater.* **2009**, *19*, 215–222.
4. Liong, M.; Lu, J.; Kovochich, M.; Xia, T.; Ruehm, S. G.; Nel, A. E.; Tamanoi, F.; Zink, J. I. Multifunctional Inorganic Nanoparticles for Imaging, Targeting, and Drug Delivery. *ACS Nano* **2008**, *2*, 889–896.
5. Meng, H.; Liong, M.; Xia, T.; Li, Z.; Ji, Z.; Zink, J. I.; Nel, A. E. Engineered Design of Mesoporous Silica Nanoparticles to Deliver Doxorubicin and P-Glycoprotein siRNA to Overcome Drug Resistance in a Cancer Cell Line. *ACS Nano* **2010**, *4*, 4539–4550.
6. Meng, H.; Xue, M.; Xia, T.; Zhao, Y.-L.; Tamanoi, F.; Stoddart, J. F.; Zink, J. I.; Nel, A. E. Autonomous *in Vitro* Anticancer Drug Release from Mesoporous Silica Nanoparticles by pH-Sensitive Nanovalves. *J. Am. Chem. Soc.* **2010**, *132*, 12690–12697.
7. Xia, T.; Kovochich, M.; Liong, M.; Meng, H.; Kabehie, S.; George, S.; Zink, J. I.; Nel, A. E. Polyethyleneimine Coating Enhances the Cellular Uptake of Mesoporous Silica Nanoparticles and Allows Safe Delivery of siRNA and DNA Constructs. *ACS Nano* **2009**, *3*, 3273–3286.
8. Radu, D. R.; Lai, C.-Y.; Jeftinija, K.; Rowe, E. W.; Jeftinija, S.; Lin, V. S. Y.; Polyamidoamine Dendrimer-Capped, A Mesoporous Silica Nanosphere-Based Gene Transfection Reagent. *J. Am. Chem. Soc.* **2004**, *126*, 13216–13217.
9. Slowing, I. I.; Trewyn, B. G.; Lin, V. S. Y. Mesoporous Silica Nanoparticles for Intracellular Delivery of Membrane-Impermeable Proteins. *J. Am. Chem. Soc.* **2007**, *129*, 8845–8849.
10. Lee, C.-H.; Cheng, S.-H.; Huang, I. P.; Souris, J. S.; Yang, C.-S.; Mou, C.-Y.; Lo, L.-W. Intracellular pH-Responsive Mesoporous Silica Nanoparticles for the Controlled Release of Anticancer Chemotherapeutics. *Angew. Chem., Int. Ed.* **2010**, *49*, 8214–8219.
11. Liu, T.; Li, L.; Teng, X.; Huang, X.; Liu, H.; Chen, D.; Ren, J.; He, J.; Tang, F. Single and Repeated Dose Toxicity of Mesoporous Hollow Silica Nanoparticles in Intravenously Exposed Mice. *Biomaterials* **2011**, *32*, 1657–1668.
12. Al Shamsi, M.; Al Samri, M. T.; Al-Salam, S.; Conca, W.; Shaban, S.; Benedict, S.; Tariq, S.; Biradar, A. V.; Penefsky, H. S.; Asefa, T.; *et al*. Biocompatibility of Calcined Mesoporous Silica Particles with Cellular Bioenergetics in Murine Tissues. *Chem. Res. Toxicol.* **2010**, *23*, 1796–1805.
13. Lu, J.; Liong, M.; Li, Z.; Zink, J. I.; Tamanoi, F. Biocompatibility, Biodistribution, and Drug-Delivery Efficiency of Mesoporous Silica Nanoparticles for Cancer Therapy in Animals. *Small* **2010**, *6*, 1794–1805.
14. Davis, M. E.; Chen, Z.; Shin, D. M. Nanoparticle Therapeutics: An Emerging Treatment Modality for Cancer. *Nat. Rev. Drug Discovery* **2008**, *7*, 771–782.
15. Nel, A. E.; Madler, L.; Velegol, D.; Xia, T.; Hoek, E. M. V.; Somasundaran, P.; Klaessig, F.; Castranova, V.; Thompson, M. Understanding Biophysicochemical Interactions at the Nano-Bio Interface. *Nat. Mater.* **2009**, *8*, 543–557.
16. Ruenraroengsak, P.; Cook, J. M.; Florence, A. T. Nanosystem Drug Targeting: Facing up to Complex Realities. *J. Controlled Release* **2010**, *141*, 265–276.
17. de Wolf, H. K.; Snel, C. J.; Verbaan, F. J.; Schiffelers, R. M.; Hennink, W. E.; Storm, G. Effect of Cationic Carriers on the Pharmacokinetics and Tumor Localization of Nucleic Acids After Intravenous Administration. *Int. J. Pharm.* **2007**, *331*, 167–175.
18. Nie, S.; Xing, Y.; Kim, G. J.; Simons, J. W. Nanotechnology Applications in Cancer. *Annu. Rev. Biomed. Eng.* **2007**, *9*, 12.1–12.32.
19. Perrault, S. D.; Walkey, C.; Jennings, T.; Fischer, H. C.; Chan, W. C. W. Mediating Tumor Targeting Efficiency of Nanoparticles Through Design. *Nano Lett.* **2009**, *9*, 1909–1915.
20. Ferrari, M. Cancer Nanotechnology: Opportunities and Challenges. *Nat. Rev. Cancer* **2005**, *5*, 161–171.
21. Maeda, H.; Bharate, G. Y.; Daruwalla, J. Polymeric Drugs for Efficient Tumor-Targeted Drug Delivery Based on EPR-effect. *Eur. J. Pharm. Biopharm.* **2009**, *71*, 409–419.
22. Torchilin, V. Tumor Delivery of Macromolecular Drugs Based on the EPR Effect. *Adv. Drug Delivery Rev.* **2011**, *63*, 131–135.
23. Iyer, A. K.; Khaled, G.; Fang, J.; Maeda, H. Exploiting the Enhanced Permeability and Retention Effect for Tumor Targeting. *Drug Discovery Today* **2006**, *11*, 812–818.
24. Lee, H.; Fonge, H.; Hoang, B.; Reilly, R. M.; Allen, C. The Effects of Particle Size and Molecular Targeting on the Intratumoral and Subcellular Distribution of Polymeric Nanoparticles. *Mol. Pharmaceutics* **2010**, *7*, 1195–1208.
25. Cho, K.; Wang, X.; Nie, S.; Chen, Z.; Shin, D. M. Therapeutic Nanoparticles for Drug Delivery in Cancer. *Clin. Cancer Res.* **2008**, *14*, 1310–1316.
26. Maeda, H.; Kabanov, A.; Kataoka, K.; Okano, T.; Fang, J.; Sawa, T.; Maeda, H., Factors and Mechanism of "EPR" Effect and the Enhanced Antitumor Effects of Macromolecular Drugs Including SMANCS. In *Polymer Drugs in the Clinical Stage*; Springer US, 2004; Vol. 519, pp 29−49.
27. Frangioni, J. V. *In Vivo* Near-Infrared Fluorescence Imaging. *Curr. Opin. Chem. Biol.* **2003**, *7*, 626–634.
28. Farist, F.; Thornileyt, M.; Wickramasinghet, Y.; Houstont, R.; Rolfet, P.; Livers, N.; Spencer, A. Non-Invasive *In Vivo* Near-infrared Optical Measurement of the Penetration Depth in the Neonatal Head. *Clin. Phys. Phgsiol. Meas.* **1991**, *12*, 353–358.
29. Bettio, A.; Honer, M.; Muller, C.; Bruhlmeier, M.; Muller, U.; Schibli, R.; Groehn, V.; Schubiger, A. P.; Ametamey, S. M. Synthesis and Preclinical Evaluation of a Folic Acid Derivative Labeled with ^{18}F for PET Imaging of Folate Receptor-Positive Tumors. *J. Nucl. Med.* **2006**, *47*, 1153–1160.
30. Kaul, G.; Amiji, M. Biodistribution and Targeting Potential of Poly(Ethylene Glycol)-Modified Gelatin Nanoparticles in Subcutaneous Murine Tumor Model. *J. Drug Target* **2004**, *12*, 585–591.
31. Verbaan, F. J.; Oussoren, C.; Snel, C. J.; Crommelin, D. J. A.; Hennink, W. E.; Storm, G. Steric Stabilization of Poly-(2-(Dimethylamino)Ethyl Methacrylate)-Based Polyplexes Mediates Prolonged Circulation and Tumor Targeting in Mice. *J. Gene Med.* **2004**, *6*, 64–75.
32. Fenske, D.; MacLachlan, I.; Cullis, P. Long-Circulating Vectors for the Systemic Delivery of Genes. *Curr. Opin. Mol. Ther.* **2001**, *3*, 153–158.
33. Gamen, S.; Anel, A.; Pérez-Galán, P.; Lasierra, P.; Johnson, D.; Piñeiro, A.; Naval, J. Doxorubicin Treatment Activates a Z-VAD-Sensitive Caspase, Which Causes Deltapsim Loss, Caspase-9 Activity, and Apoptosis in Jurkat Cells. *Exp. Cell Res.* **2000**, *258*, 223–235.
34. Garg, A.; Misra, A. Hepatic Steatosis, Insulin Resistance, and Adipose Tissue Disorders. *J. Clin. Endocrinol. Metab.* **2002**, *87*, 3019–3022.
35. Nomura, R.; Ishizaki, Y.; Suzuki, K.; Kawasaki, S. Development of Hepatic Steatosis After Pancreatoduodenectomy. *Am. J. Roentgenol.* **2007**, *189*, 1484–1488.
36. Kandutsch, S.; Klinger, M.; Hacker, S.; Wrba, F.; Gruenberger, B.; Gruenberger, T. Patterns of Hepatotoxicity After Chemotherapy for Colorectal Cancer Liver Metastases. *Eur. J. Surg. Oncol.* **2008**, *34*, 1231–1236.
37. Yagmurca, M.; Erdogan, H.; Iraz, M.; Songur, A.; Ucar, M.; Fadillioglu, E. Caffeic Acid Phenethyl Ester as a Protective Agent Against Doxorubicin Nephrotoxicity in Rats. *Clin. Chim. Acta* **2004**, *348*, 27–34.
38. Arola, O. J.; Saraste, A.; Pulkki, K.; Kallajoki, M.; Parvinen, M.; Voipio-Pulkki, L.-M. Acute Doxorubicin Cardiotoxicity

Involves Cardiomyocyte Apoptosis. *Cancer Res.* **2000**, *60*, 1789–1792.
39. Slowing, I. I.; Wu, C. W.; Vivero-Escoto, J. L.; Lin, V. S. Y. Mesoporous Silica Nanoparticles for Reducing Hemolytic Activity Towards Mammalian Red Blood Cells. *Small* **2009**, *5*, 57–62.
40. Kursa, M.; Walker, G. F.; Roessler, V.; Ogris, M.; Roedl, W.; Kircheis, R.; Wagner, E. Novel Shielded Transferrin Polyethylene Glycol Polyethylenimine/DNA Complexes for Systemic Tumor-Targeted Gene Transfer. *Bioconjugate Chem.* **2002**, *14*, 222–231.
41. Kircheis, R.; Ostermann, E.; Wolschek, M. F.; Lichtenberger, C.; Magin-Lachmann, C.; Wightman, L.; Kursa, M.; Wagner, E. Tumor-Targeted Gene Delivery of Tumor Necrosis Factor-[Alpha] Induces Tumor Necrosis And Tumor Regression Without Systemic Toxicity. *Cancer Gene. Ther.* **2002**, *9*, 673–680.
42. Febvay, S.; Marini, D. M.; Belcher, A. M.; Clapham, D. E. Targeted Cytosolic Delivery of Cell-Impermeable Compounds by Nanoparticle-Mediated, Light-Triggered Endosome Disruption. *Nano Lett.* **2010**, *10*, 2211–2219.
43. Petersen, H.; Fechner, P. M.; Martin, A. L.; Kunath, K.; Stolnik, S.; Roberts, C. J.; Fischer, D.; Davies, M. C.; Kissel, T. Polyethylenimine-graft-Poly(ethylene glycol) Copolymers: Influence of Copolymer Block Structure on DNA Complexation and Biological Activities as Gene Delivery System. *Bioconjugate Chem.* **2002**, *13*, 845–854.
44. Tang, G. P.; Zeng, J. M.; Gao, S. J.; Ma, Y. X.; Shi, L.; Li, Y.; Too, H. P.; Wang, S. Polyethylene Glycol Modified Polyethylenimine for Improved CNS Gene Transfer: Effects of PEGylation Extent. *Biomaterials* **2003**, *24*, 2351–2362.
45. Kunath, K.; von Harpe, A.; Petersen, H.; Fischer, D.; Voigt, K.; Kissel, T.; Bickel, U. The Structure of PEG-Modified Poly-(Ethylene Imines) Influences Biodistribution and Pharmacokinetics of Their Complexes with NF-κB Decoy in Mice. *Pharm. Res.* **2002**, *19*, 810–817.
46. Zhang, S.; Kucharski, C.; Doschak, M. R.; Sebald, W.; Uludag, H. Polyethylenimine-PEG Coated Albumin Nanoparticles for BMP-2 Delivery. *Biomaterials* **2010**, *31*, 952–963.
47. Kawano, T.; Yamagata, M.; Takahashi, H.; Niidome, Y.; Yamada, S.; Katayama, Y.; Niidome, T. Stabilizing of Plasmid DNA *In Vivo* by PEG-Modified Cationic Gold Nanoparticles and the Gene Expression Assisted with Electrical Pulses. *J. Controlled Release* **2006**, *111*, 382–389.
48. Thierry, B.; Zimmer, L.; McNiven, S.; Finnie, K.; Barbe, C.; Griesser, H. J. Electrostatic Self-Assembly of PEG Copolymers onto Porous Silica Nanoparticles. *Langmuir* **2008**, *24*, 8143–8150.
49. Fang, J.; Nakamura, H.; Maeda, H. The EPR Effect: Unique Features of Tumor Blood Vessels for Drug Delivery, Factors Involved, and Limitations and Augmentation of the Effect. *Adv. Drug Delivery Rev.* **2011**, *63*, 136–151.
50. Suzuki, M.; Hori, K.; Abe, I.; Saito, S.; Sato, H. A New Approach to Cancer Chemotherapy: Selective Enhancement of Tumor Blood Flow With Angiotensin II. *J. Natl. Cancer Inst.* **1981**, *67*, 663–669.
51. Seki, T.; Fang, J.; Maeda, H. Enhanced Delivery of Macromolecular Antitumor Drugs to Tumors by Nitroglycerin Application. *Cancer Sci.* **2009**, *100*, 2426–2430.
52. Minko, T.; Kopečkova, P.; Pozharov, V.; Jensen, K. D.; Kopeček, J. The Influence of Cytotoxicity of Macromolecules and of VEGF Gene Modulated Vascular Permeability on the Enhanced Permeability and Retention Effect in Resistant Solid Tumors. *Pharm. Res.* **2000**, *17*, 505–514.
53. Sugahara, K. N.; Teesalu, T.; Karmali, P. P.; Kotamraju, V. R.; Agemy, L.; Greenwald, D. R.; Ruoslahti, E. Coadministration of a Tumor-Penetrating Peptide Enhances the Efficacy of Cancer Drugs. *Science* **2010**, *328*, 1031–1035.
54. Maeda, H. Tumor-Selective Delivery of Macromolecular Drugs *via* the EPR Effect: Background and Future Prospects. *Bioconjugate Chem.* **2010**, *21*, 797–802.
55. Mao, S.; Germershaus, O.; Fischer, D.; Linn, T.; Schnepf, R.; Kissel, T. Uptake and Transport of PEG-Graft-Trimethyl-Chitosan Copolymer-Insulin Nanocomplexes by Epithelial Cells. *Pharm. Res.* **2005**, *22*, 2058–2068.
56. Zhang, H.; Xia, T.; Meng, H.; Xue, M.; George, S.; Ji, Z.; Wang, X.; Liu, R.; Wang, M.; France, B.; *et al*. Differential Expression of Syndecan-1 Mediates Cationic Nanoparticle Toxicity in Undifferentiated versus Differentiated Normal Human Bronchial Epithelial Cells. *ACS Nano* 2011, 10.1021/nn200328m.
57. Portney, N.; Ozkan, M. Nano-Oncology: Drug Delivery, Imaging, and Sensing. *Anal. Bioanal. Chem.* **2006**, *384*, 620–630.
58. Vallet-Regi, M.; Ramila, A.; del Real, R. P.; Perez-Pariente, J. A New Property of MCM-41: Drug Delivery System. *Chem. Mater.* **2000**, *13*, 308–311.
59. Hayek, E. R.; Speakman, E.; Rehmus, E. Acute Doxorubicin Cardiotoxicity. *N. Engl. J. Med.* **2005**, *352*, 2456–2457.
60. Li, S.-D.; Huang, L. Pharmacokinetics and Biodistribution of Nanoparticles. *Mol. Pharmaceutics* **2008**, *5*, 496–504.
61. Souris, J. S.; Lee, C.-H.; Cheng, S.-H.; Chen, C.-T.; Yang, C.-S.; Ho, J.-a. A.; Mou, C.-Y.; Lo, L.-W. Surface Charge-Mediated Rapid Hepatobiliary Excretion of Mesoporous Silica Nanoparticles. *Biomaterials* **2010**, *31*, 5564–5574.
62. Noguchi, Y.; Wu, J.; Duncan, R.; Strohalm, J.; Ulbrich, K.; Akaike, T.; Maeda, H. Early Phase Tumor Accumulation of Macromolecules: A Great Difference in Clearance Rate between Tumor and Normal Tissues. *Cancer Sci.* **1998**, *89*, 307–314.
63. Cauda, V.; Schlossbauer, A.; Bein, T. Bio-Degradation Study of Colloidal Mesoporous Silica Nanoparticles: Effect of Surface Functionalization with Organo-Silanes and Poly-(Ethylene Glycol). *Microporous Mesoporous Mater.* **2010**, *132*, 60–71.
64. Meng, H.; Xing, G.; Sun, B.; Zhao, F.; Lei, H.; Li, W.; Song, Y.; Chen, Z.; Yuan, H.; Wang, X.; *et al*. Potent Angiogenesis Inhibition by the Particulate Form of Fullerene Derivatives. *ACS Nano* **2010**, *4*, 2773–2783.